

REYNOLDS AND MACH NUMBER EFFECTS ON MULTIELEMENT AIRFOILS

219-02
160479

Walter O. Valarezo*, Chet J. Dominik**
Aerodynamics Technology
Douglas Aircraft Company

N 9 3 - 27¹³ 4 4 6

and

Robert J. McGhee*
Experimental Flow Physics Branch
NASA Langley Research Center

Abstract

Experimental studies have been conducted to assess Reynolds and Mach number effects on a supercritical multielement airfoil. The airfoil is representative of the stall-critical station of an advanced transport wing design. The experimental work was conducted as part of a cooperative program between the Douglas Aircraft Company and the NASA Langley Research Center to improve current knowledge of high-lift flows and to develop a validation database with practical geometries/conditions for emerging computational methods. This paper describes results obtained for both landing and takeoff multielement airfoils (four and three-element configurations) for a variety of Mach/Reynolds number combinations up to flight conditions. Effects on maximum lift are considered for the landing configurations and effects on both lift and drag are reported for the takeoff geometry. The present test results revealed considerable maximum lift effects on the three-element landing configuration for Reynolds number variations and significant Mach number effects on the four-element airfoil.

Nomenclature

C_d	Drag Coefficient
C_l	Lift Coefficient
$C_{l,max}$	Maximum Lift Coefficient
C_p	Pressure Coefficient
L/D	Lift-to-Drag Ratio
M	Mach Number
RN	Chord Reynolds Number
α	Angle of Attack
δ_f	Flap Deflection
δ_s	Slat Deflection

Introduction

Commercial transport aircraft wings are configured with leading-edge slats and trailing-edge flaps to meet takeoff and landing operational requirements. High-Lift systems have traditionally been complex in order to attain the aerodynamic capability of generating high L/D in climb and high maximum lift on approach. However, increased financial pressures in the airline business demand high-lift wing designs that are simpler and easier to maintain while achieving improved aerodynamic performance over previous-generation designs. A major obstacle in the design process towards more efficient multielement airfoils has been the lack of published data on the effects of Reynolds and Mach number over a realistic range for representative multielement airfoils. This lack of data is also likely to have delayed the development of computational methods

* Principal Technical Specialist
Team Leader-Subsonics & High Lift
** Engineer/Scientist.
* Section Head, Low-Turbulence Pressure Tunnel

suitable for the analysis of practical multi-element airfoils at conditions of interest (maximum lift). Several purely computational methods have been recently reported in the literature¹⁻¹⁰ that can handle, to various degrees of success, the viscous flow over multi-element airfoils. However, these methods have largely been applied to either geometries that are not really representative of transport high lift airfoils or to flow conditions that do not include maximum lift. It is expected that some of these methods (either Navier-Stokes or boundary-layer based) hold significant promise but may not be substantially improved by their developers in the absence of a quality database at realistic conditions for a practical airfoil. The work reported in this paper is the result of a cooperative experimental program conducted by the Douglas Aircraft Company and the NASA Langley Research Center to establish a database for Reynolds and Mach number (including flight condition) effects on the flow over transport multi-element airfoils.

Test Facility and Model Description

The Langley Low Turbulence Pressure Tunnel (LTPT) is a single return, closed-throat wind tunnel that can be operated up to 10 atmospheres thus allowing very high Reynolds number capability¹¹ (Fig. 1). The test section is 3 feet wide by 7.5 feet high by 7.5 feet long. To promote two-dimensional flow over the model in view of its low aspect ratio and strong wall-model aerodynamic interference, a new side-wall boundary layer control (BLC) system was installed at the LTPT for the present test¹². The BLC system employed the differential pressure between the test section and the atmosphere to provide suction of the boundary layer through porous endplates. The system yielded good quality two-dimensional flow over the model for the Reynolds numbers tested¹². The model spanned the width of the test section and had a clean (stowed) airfoil chord of 22 inches. The clean airfoil and the takeoff and landing multi-element configura-

tions tested are shown in Fig. 2. The slat chord

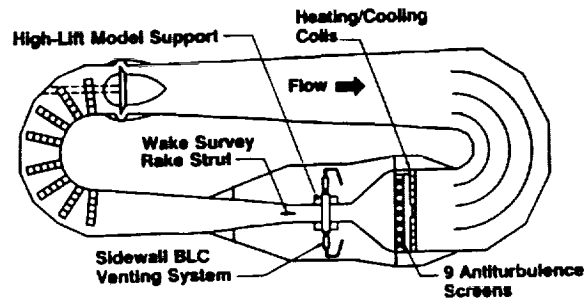


Figure 1. Schematic of Low Turbulence Pressure Tunnel

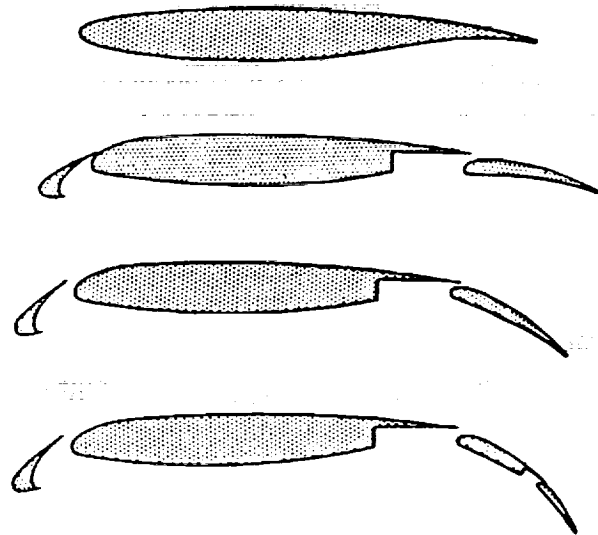


Figure 2. Airfoil Configurations Tested in the LTPT

ratio was 14.48%, the single-segment flap chord ratio was 30%, and the two-segment flap had a chord ratio of 21% for the main segment and 13% for the auxiliary flap. Pressure orifices were located along the centerline of the model (142 taps for the four-element configuration). Additionally, pressure taps were located along (or near) the trailing edge of each airfoil element to monitor two-dimensionality of the flow at run time. Integration of the pressure measurements yielded the forces presented here. The data is corrected for the effects of the sidewall suction system on the tunnel parameters and no blockage corrections were applied. Four rows of streamlined support brackets for the high-lift devices (Fig. 3)

were required due to the very high loads (up to 15,000 pounds) associated with the high freestream dynamic pressure and lift coefficients attained. Drag data were computed by integration of the static and total pressures obtained from the LTPT wake survey rake system.

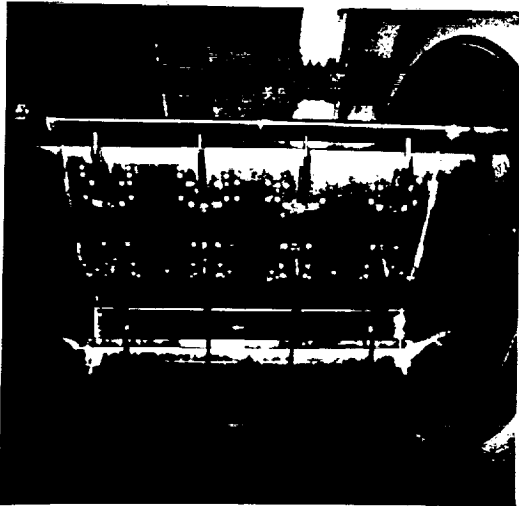


Figure 3. LTPT High-Lift Model Support Brackets

Results

A significant fraction of the wind tunnel testing associated with multielement airfoils is aimed at optimizing the rigging of a particular airfoil with fixed slat and flap chord ratios. Parameters defining rigging nomenclature for multielement airfoils are shown in Fig. 4. The optimization work is traditionally performed at a given Mach/Reynolds number that should be representative of nominal flight conditions. However, it is also very important to determine the effects on the performance of the optimized airfoil for departures in Reynolds or Mach number from the nominal conditions. It was possible to perform these measurements (Reynolds and Mach number sweeps) at the Langley Low Turbulence Pressure Tunnel because of its considerable operational capability (Fig. 5).

The application of so-called transition strips in wind tunnel testing is an attempt to simulate

the extent of turbulent flow that would naturally occur at flight Reynolds numbers on an airfoil (or wing) but not at the low

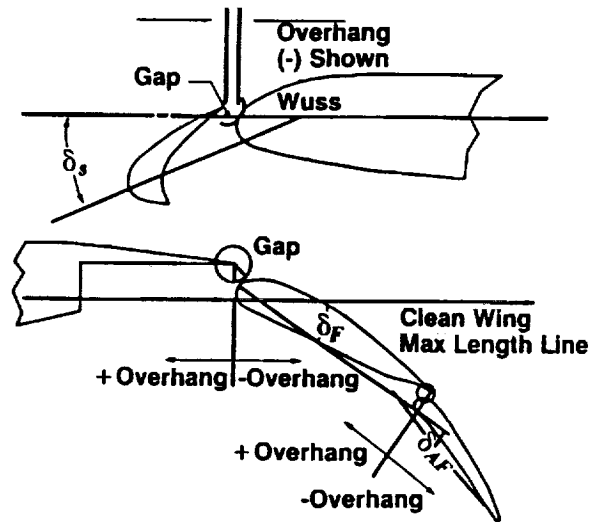


Figure 4. Nomenclature for Multielements

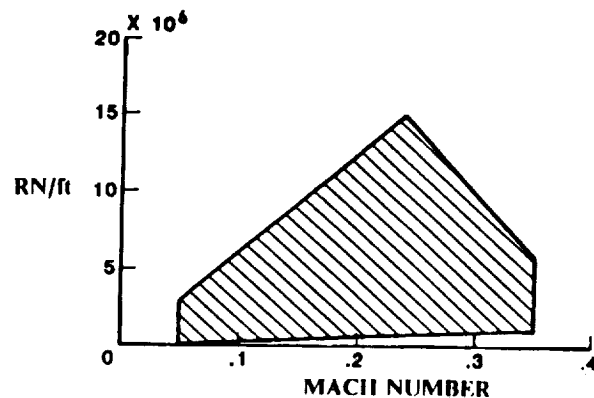


Figure 5. Operational Capability of the LTPT

wind tunnel Reynolds numbers typically attainable. Hence, in a facility such as the LTPT where flight Reynolds can actually be achieved it is not necessary to attempt to simulate transition on the airfoil. Additionally, the low turbulence level achieved in the test section increases the applicability of results obtained at a given Reynolds number since this is more representative of flight conditions. The accurate modeling of transition over a wide range of angles-of-attack, Reynolds/Mach number combinations, and multiple airfoil elements is not practical. All results shown here were obtained transition-free.

The effects of Reynolds number on the clean airfoil maximum lift capability at various Mach numbers is shown in Fig. 6. It can be seen that there is a considerable increase in maximum lift between Reynolds numbers of 2.5×10^6 and 9×10^6 . Corresponding surface pressures on the clean airfoil at maximum lift are shown in Figs 7-10. The effects of Mach number on maximum lift are shown in Fig. 11 for Reynolds numbers from 5 to 18×10^6 . It can be seen that the effect of Mach number is substantially more pronounced at the lower Reynolds numbers. Lifts curves at 5×10^6 and 9×10^6 are shown in Figs. 12 and 13 where Mach number can be seen to affect the stall angle as well.

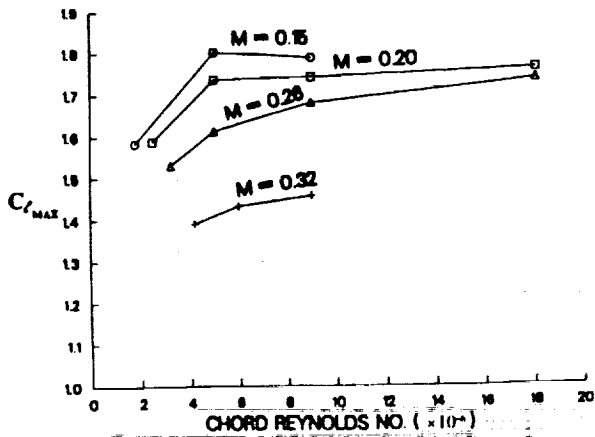


Figure 6. Reynolds Number Effect on Maximum Lift.

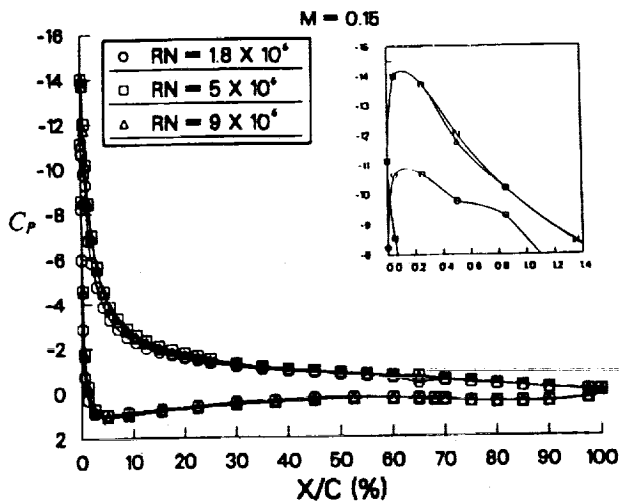


Figure 7. Reynolds Number Effect at Maximum Lift.

These results shown for the basic clean airfoil (Figs. 6-13) served to establish a baseline for both Reynolds and Mach number effects for the subsequent multielement airfoil measurements and they may also represent a logical starting point for the validation of any viscous flow method since surface grid complications are at a practical minimum and flow features through the maximum lift condition are still complex enough to be of interest.

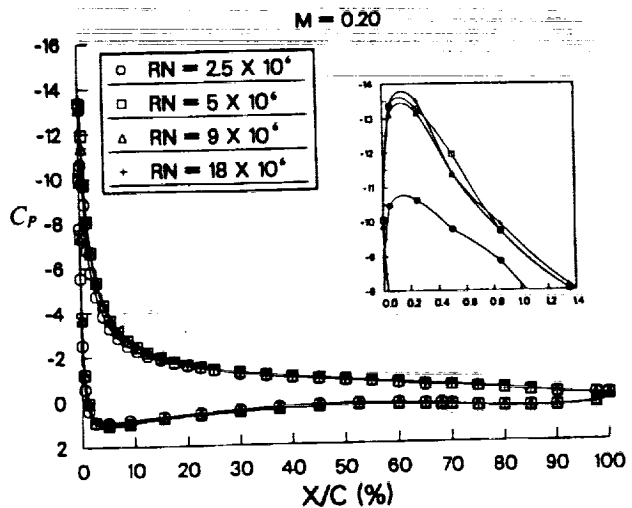


Figure 8. Reynolds Number Effect at Maximum Lift.

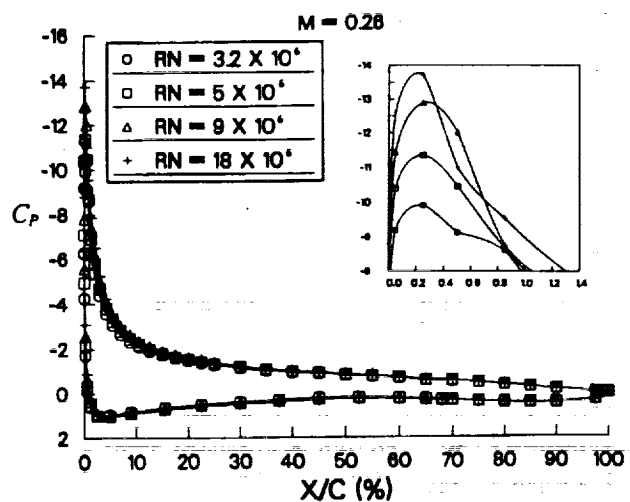


Figure 9. Reynolds Number Effect at Maximum Lift.

C-3

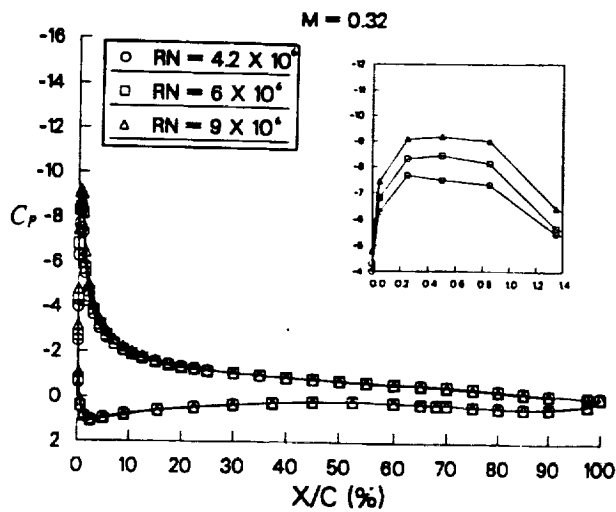


Figure 10. Reynolds Number Effect at Maximum Lift.

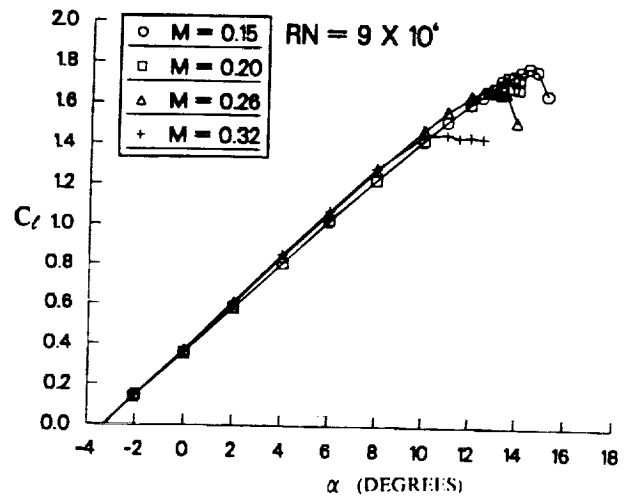


Figure 13. Mach Number Effect on Lift.

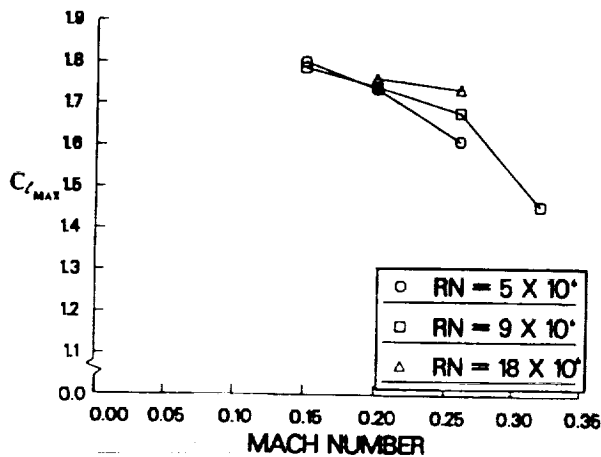


Figure 11. Mach Number Effect on Maximum Lift.

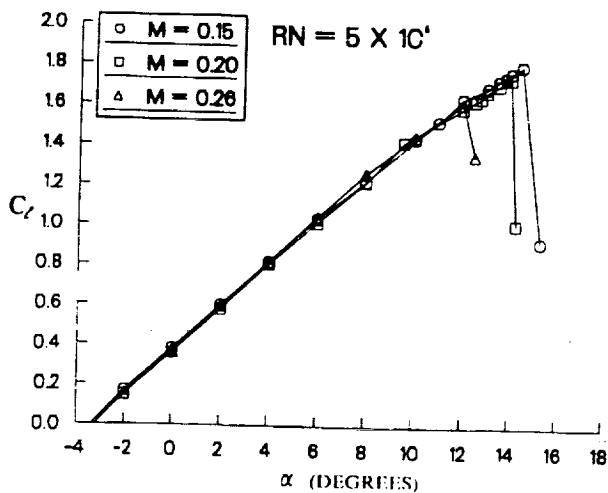


Figure 12. Mach Number Effect on Lift.

Takeoff Configuration

A three-element airfoil configured for takeoff was tested at various combinations of Reynolds and Mach number as shown below:

Freestream Mach Number

	0.15	0.20	0.26	0.30	0.32
5	x	x	x	x	
9	x	x	x	x	x
16	x	x			
20		x			

The slat deflection was 20° (gap = 0.55%, overhang = + 1.0%), and the flap was rigged at a gap of 1.82%, overhang of 1.5%, and 10° of deflection. For a takeoff configuration the slat is normally sealed (gap = 0%) to minimize profile drag, however, an open slat was chosen for this study since it should be less difficult to grid from a computational analysis perspective. Additionally, this particular open slat configuration yielded takeoff performance close to that of a sealed slat at a representative lift coefficient.

Lift curves and drag polars for Reynolds numbers from 5 to 16×10^6 at Mach 0.15 are shown in Fig. 14. There is a loss in maximum lift and improved drag performance with increasing Reynolds number. It is also interesting to note that while the main element enters the stall first, it is soon followed by the slat and not the flap. In fact, the flap lift coefficient increases after the stall. This effect appears to be due to the drastically reduced downwash from both the slat and the main element and the fact that the geometric deflection of the flap (10°) is not enough by itself to cause the flow on the flap to separate. Reynolds number effects on lift and drag obtained at Mach 0.20 are shown in Fig. 15. Here, it is evident that the Reynolds number effect is largely on drag and not on lift. Differences in measured drag are approximately 10% between 5×10^6 and 20×10^6 Reynolds number. Again, the flap loads up after the main element and the slat enter the stall. In fact, it is now clear that the flap loads up after the slat stalls. Results at Mach 0.26 and 0.30 are shown in Figs. 16 and 17, respectively. At these two Mach numbers the Reynolds number effect is to increase maximum lift (opposite trend from Mach 0.15) but, in general, the Reynolds number effect on either lift or drag is minimal. It is worth noting that at these conditions even though the main element exhibits a pronounced stall, the slat does not, and the flap displays only a slight tendency to load up beyond the stall. That the slat does not really stall, as it did at lower Mach numbers, is a result of the slat being exposed to a lower geometric angle-of-attack (lower airfoil stall angles at higher Mach numbers). Mach number effects on the takeoff configuration at Reynolds numbers of 5×10^6 , 9×10^6 , and 16×10^6 are shown in Figs. 18, 19, and 20, respectively. Overall, the measured effect of Mach number on C_d at a given Reynolds number can be seen to be in the scatter band of the data (within 10 counts). However, the Mach effect on lift is substantial.

Landing Configurations

Two landing configurations were selected for Reynolds and Mach number effects studies. The leading-edge slat was optimized for both configurations and was positioned at a gap of 2.95% with an overhang of -2.5% and 30° of deflection.

The single-segment flap airfoil was configured with the flap optimized at a Reynolds number of 9×10^6 at 30° of deflection with a gap of 1.32% and an overhang of +1.0%. A Reynolds number sweep was conducted at Mach 0.20 and effects on maximum lift are shown in Fig. 21. There is a considerable loss in $C_{l_{max}}$ (~ 0.1) at Reynolds numbers other than 9×10^6 . Total and component loadings are shown in Fig. 22 where it can be seen again that the airfoil stall is caused by the main element. Unlike the takeoff cases reviewed above, the slat continues to load up beyond the airfoil stall. This is possibly due to the slat position being aerodynamically underdeflected (-10°) with respect to the takeoff slat discussed. Surface pressure measurements obtained at the three Reynolds numbers at maximum lift are shown in Fig. 23. Although the data are closely matched, being able to discern a difference of 0.10 in $C_{l_{max}}$ performance is of considerable importance in transport high-lift aerodynamics.

The second landing arrangement tested was a four-element airfoil with a two-segment flap. The optimum slat position was the same as for the three-element landing airfoil. The main flap was optimized at 35° with a gap of 2.9% and an overhang of -1%. The auxiliary flap was deflected an additional 15° and had a non-optimized gap of 0.68% and an overhang of 0.75%. Reynolds number effects at 0.20 Mach number are shown in Fig. 24. It is evident that the effects of Reynolds number on maximum lift are minimal for the Reynolds number range tested. This can be contrasted with the substantial Reynolds number effects shown for the

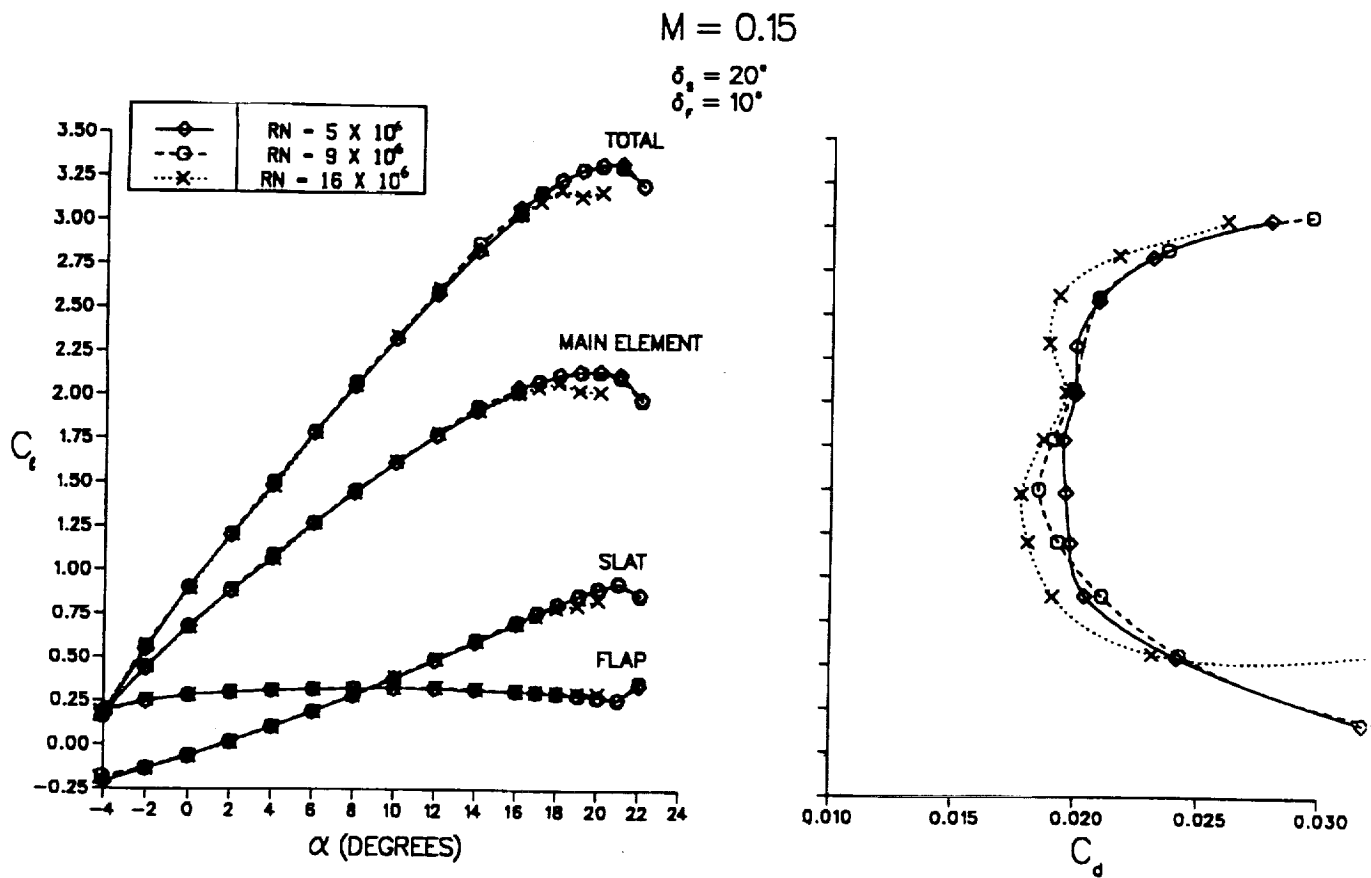


Figure 14. Reynolds Number Effect

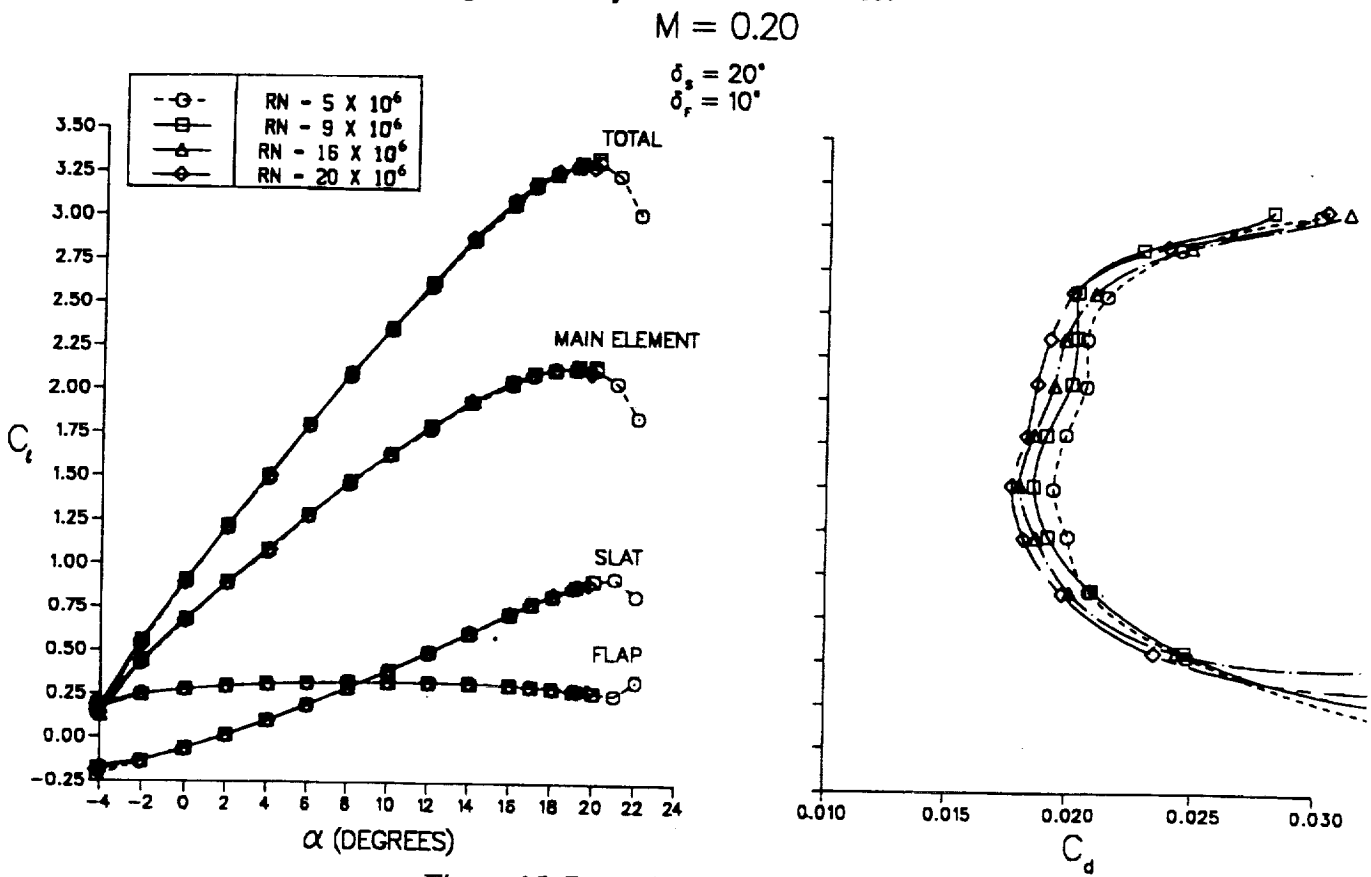


Figure 15. Reynolds Number Effect

$M = 0.26$

$\delta_s = 20^\circ$
 $\delta_r = 10^\circ$

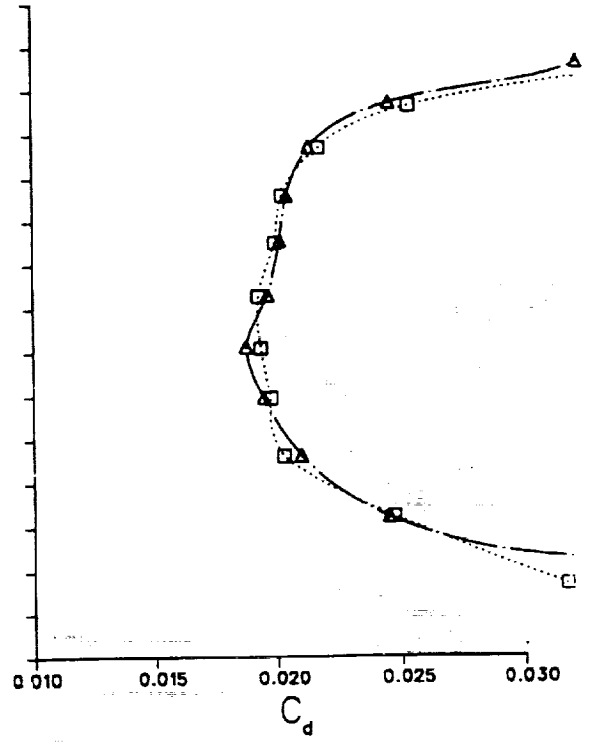
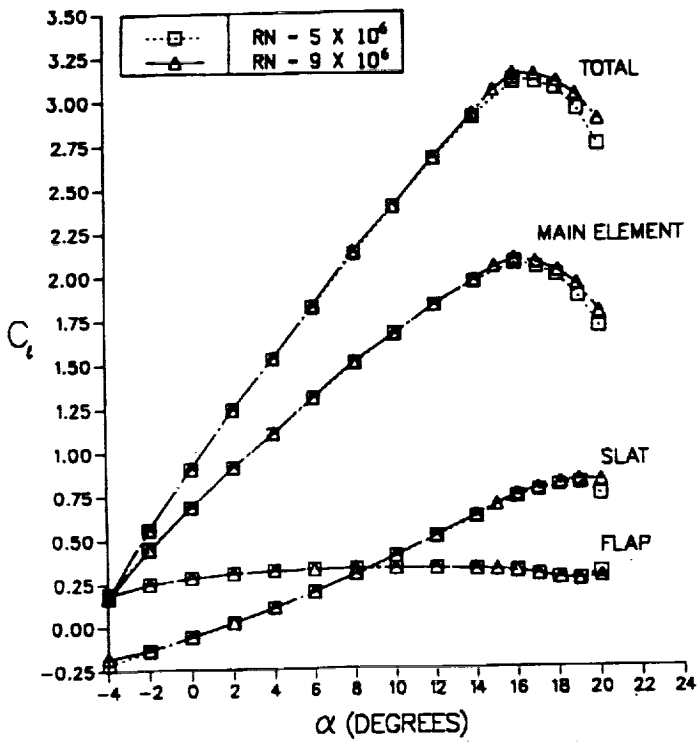


Figure 16. Reynolds Number Effect

$M = 0.30$

$\delta_s = 20^\circ$
 $\delta_r = 10^\circ$

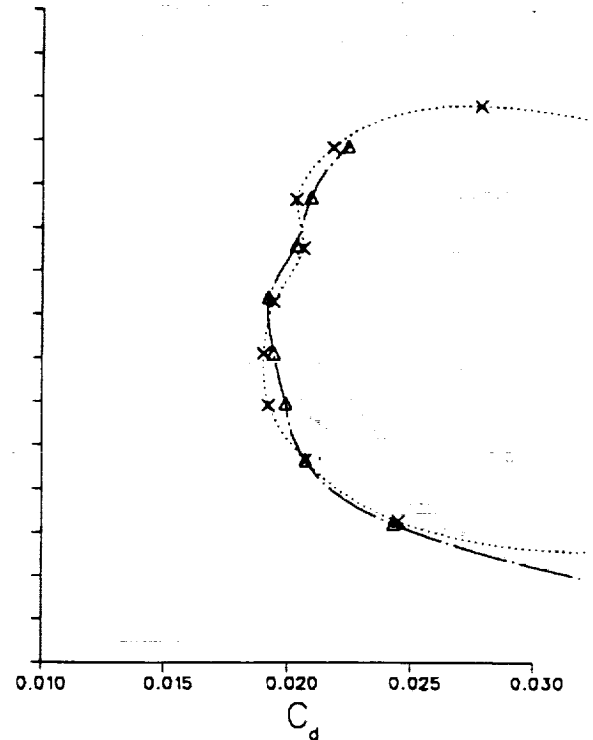
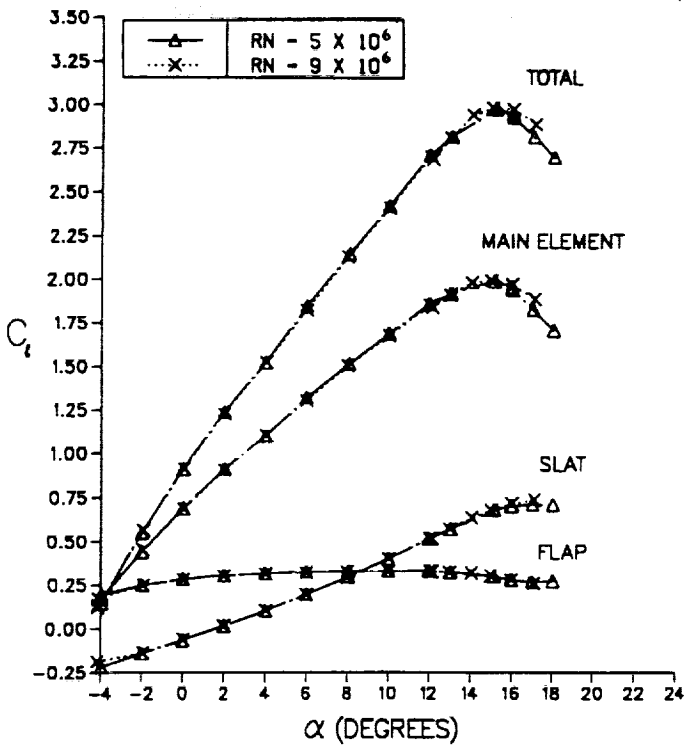


Figure 17. Reynolds Number Effect

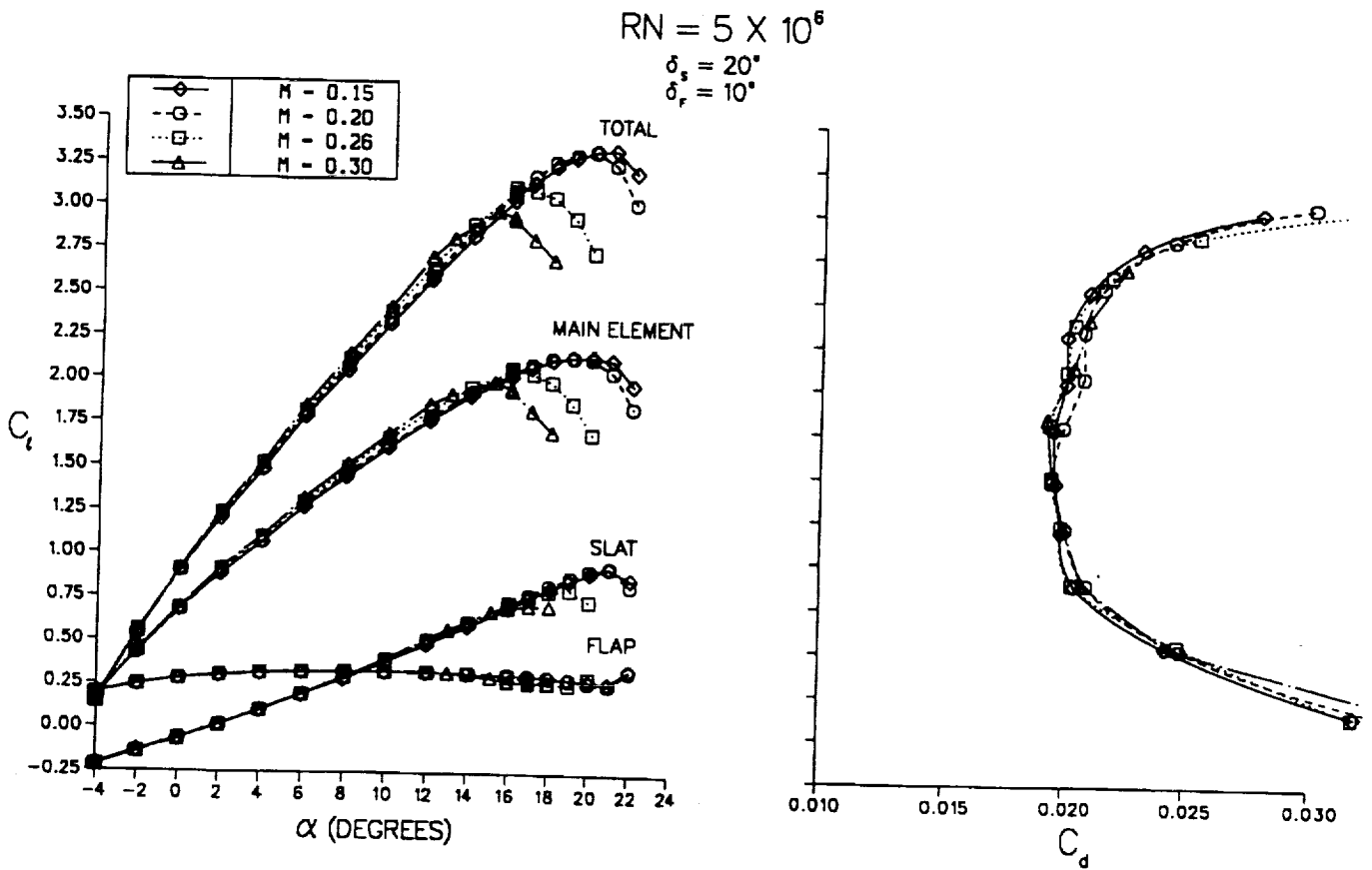


Figure 18. Mach Number Effect

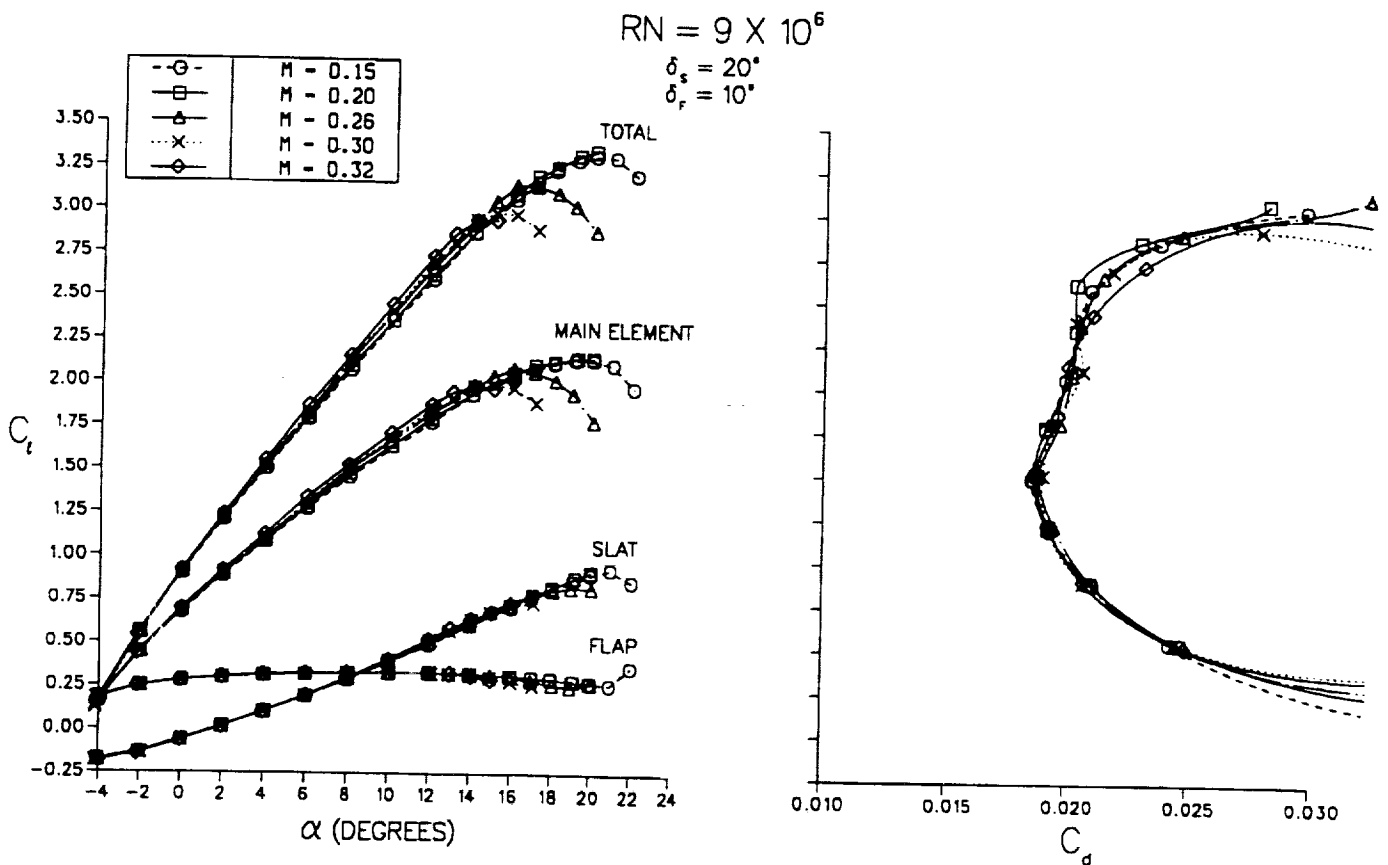


Figure 19. Mach Number Effect

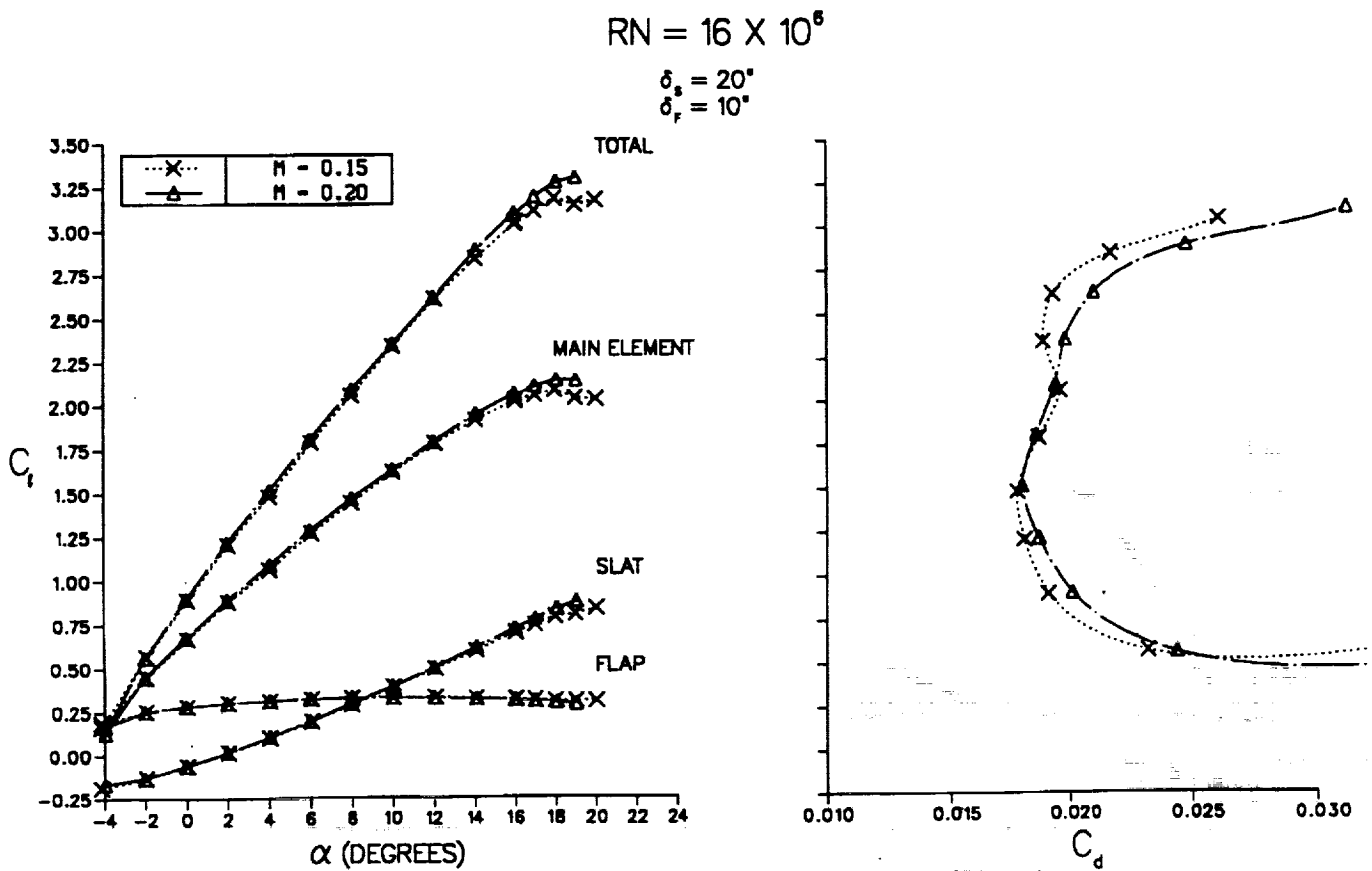


Figure 20. Mach Number Effect

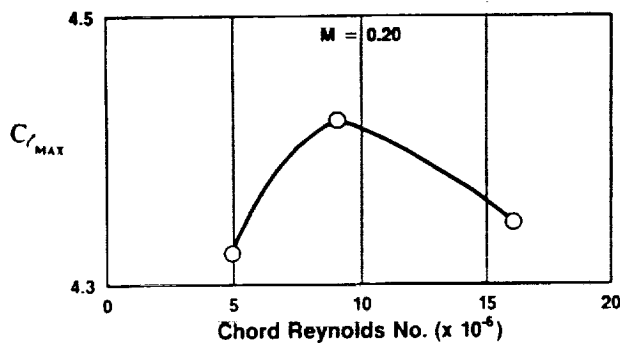


Figure 21. Reynolds Number Effect on Configuration Optimized at $RN = 9 \times 10^6$ ($\delta_s = 30^\circ$, $\delta_f = 30^\circ$)

single-segment flap configuration. It is possible that this difference in dependence on Reynolds number could be due to the large optimum gap for the two-segment flap and the much smaller (approximately half) optimum gap for a single-segment flap. These different gaps represent different enough slot geometries between the main element and the flap which could lead one configuration (single-segment flap) to be more Reynolds number sensitive

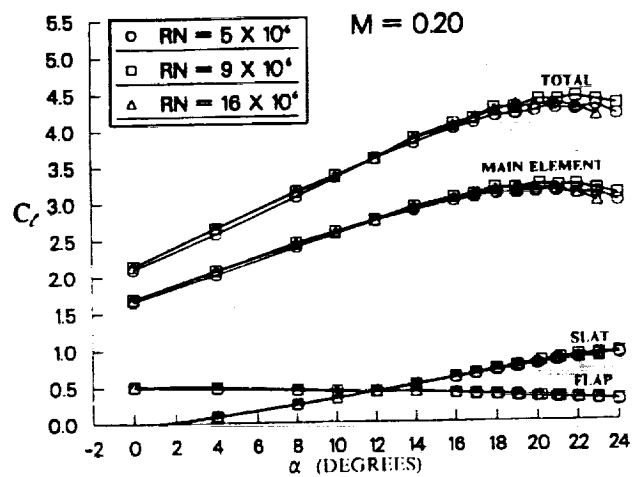


Figure 22. Reynolds Number Effect on Lift ($\delta_s = 30^\circ$, $\delta_f = 30^\circ$)

than the other. Total and component loadings are shown in Fig. 25 and the corresponding surface pressures at maximum lift are shown in Fig. 26. It is interesting to note from Fig. 25 that there is a reduction in stall angle with increased Reynolds number for this four-element configuration. This stall angle reduction trend was not as apparent for the three-

element airfoil. The effect of Mach number on maximum lift at a Reynolds number of 9×10^6 is shown in Fig. 27. Total and component loadings are shown in Fig. 28. It can be seen that increasing Mach number causes reductions in both maximum lift and stall angle.

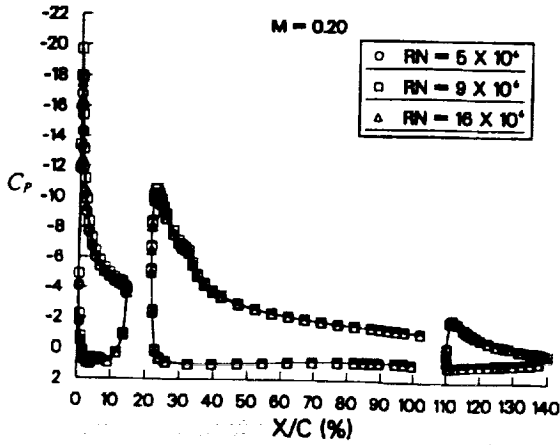


Figure 23. Reynolds Number Effect on Maximum Lift ($\delta_s=30^\circ, \delta_f=30^\circ$)

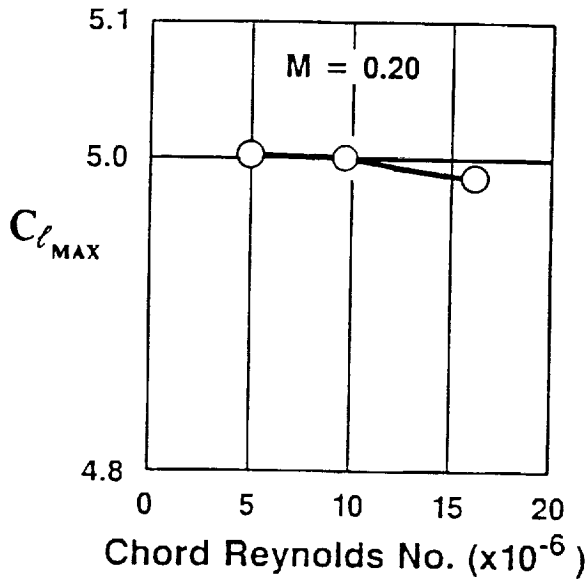


Figure 24. Reynolds Number Effect on Maximum Lift ($\delta_s=30^\circ, \delta_f=35^\circ/15^\circ$)

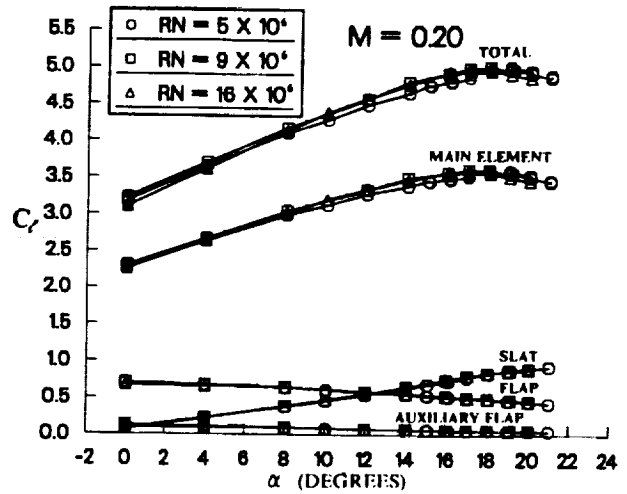


Figure 25. Reynolds Number Effect on Lift ($\delta_s=30^\circ, \delta_f=35^\circ/15^\circ$)

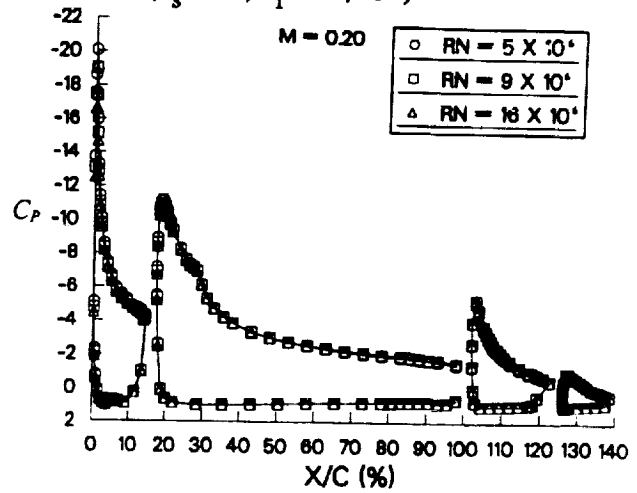


Figure 26. Reynolds Number Effect at Maximum Lift ($\delta_s=30^\circ, \delta_f=35^\circ/15^\circ$)

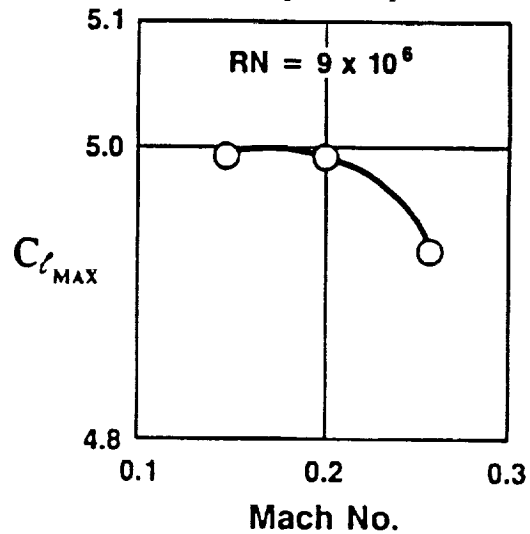


Figure 27. Mach Number Effect on Maximum Lift. ($\delta_s=30^\circ, \delta_f=35^\circ/15^\circ$)

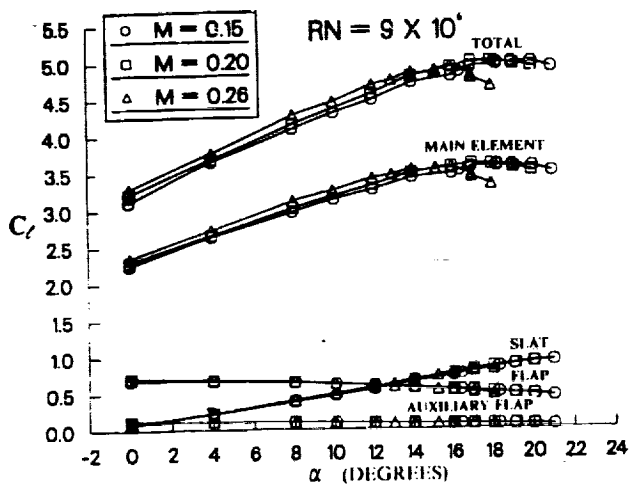


Figure 28. Mach Number Effect on Lift.
($\delta_s=30^\circ$, $\delta_f=35^\circ/15^\circ$)

Conclusions

Experimental studies of the effects of Reynolds and Mach number variations on the performance of a practical transport-type multielement high-lift airfoil have been presented. The studies were conducted at the NASA Langley Low Turbulence Pressure Tunnel under a cooperative program between the Douglas Aircraft Company and the NASA Langley Research Center to establish a high-quality database for these effects that can be used in the calibration/validation of computational methods in development for practical multielement airfoil configurations. Salient findings of the present work are:

1. Reynolds number effects are significant even on the single-element airfoil below 5×10^6 Reynolds number.
2. Mach number effects were more pronounced at the lower Reynolds numbers.
3. Extensive Reynolds and Mach number surveys were conducted on a three-element takeoff configuration ($\delta_s = 20^\circ$, $\delta_f = 10^\circ$). In general, Reynolds number effects on both lift and drag were minimal but different trends were exhibited depending on the Mach number. Mach number

effects on maximum lift were substantial.

4. For the three-element takeoff configuration the main element of the airfoil enters the stall first and is followed by the slat stalling. The flap does not stall.
5. Significant Reynolds number effects were apparent for the three-element landing configurations. As observed in the takeoff work, the main element of the airfoil stalls first. However, both the slat and flap continue to load up after the main element stalls.
6. Mach number effects on the four-element landing configuration were substantial. Reynolds number effects were not as large as those measured on the three-element airfoil. Additionally, the four-element results show a definite reduction in stall angle with increased Reynolds Number which was not apparent in either the takeoff configuration or the three-element landing configuration.

References

1. Cebeci, T., Chang, K.C., Clark, R.W., and Halsey, N. D.: Calculation of Flow Over Multielement Airfoils at High Lift. ICAS Paper No. 86-2.3.1..
2. Shima, Eiji: Numerical Analysis of Multiple Element High Lift Devices by Navier Stokes Equation Using Implicit TVD Finite Volume Method. AIAA Paper No. 88-2574-CP.
3. Wang, G., and Wu, J.: A Numerical Study of General Viscous Flows Around Multi-Element Airfoils. AIAA Paper No. 90-0572.
4. Drela, M.: Newton Solution of Coupled Viscous/Inviscid Multielement Airfoil

Flows. AIAA Paper No. 90-1470.

5. Mavriplis, D.J.: Algebraic Turbulence Modeling for Unstructured and Adaptive Meshes. NASA Contractor Report No. 182035.
6. Mavriplis, D. J.: Turbulent Flow Calculations Using Unstructured and Adaptive Meshes. NASA Contractor Report 182102.
7. Mavriplis D. J.: Multigrid Solution of Compressible Turbulent Flow on Unstructured Meshes Using a Two-Equation Model. AIAA Paper No. 91-0237.
8. Kusunose, K., Wigton, L., and Meredith, P.: A Rapidly Converging Viscous/Inviscid Coupling Code for Multi-Element Airfoil Configurations. AIAA Paper No. 91-0177.
9. Chow, R., and Chu, K.: Navier-Stokes Solution for High-Lift Multielement Airfoil System with Flap Separation. AIAA Paper No. 91 -1 623.
10. Cebeci, T., Jau, J., and Vitiello, D.: An Interactive Boundary-Layer Approach to Multielement Airfoils at High Lift. AIAA Paper No. 92-0404.
11. Valarezo, W.O., Dominik, C.J., McGhee, R.J., Goodman, W.L., and Paschal, K.B.: Multi-Element Airfoil Optimization for Maximum Lift at High Reynolds Numbers. AIAA Paper No. 91-3332.
12. Paschal, K.B., Goodman, W.L., McGhee, R.J., Walker, B., and Wilcox, P.A.: Evaluation of Tunnel Sidewall Boundary-Layer Control Systems for High-Lift Airfoil Testing. AIAA Paper No. 91 - 3243.

1950-1951

1950

1951

1952

1953

1954

1955

1956

1957

1958

1959

1960

1961

1962